43rd AIAA/ASME/SAE/ASEE Joint Propulsion Conference & Exhibit
8 - 11 July 2007, Cincinnati, OH

AIAA 2007-5240

Numerical Investigation of Electron Behavior in the Near-Field of Hall Thrusters

Andrew W. Smith[1] and Mark A. Cappelli[2]
Department of Mechanical Engineering, Plasma Physics Laboratory, Stanford University, Stanford, CA, 94043

The formulation and results of a 3-D discrete electron transport simulation are presented for the near-field of a laboratory *E* x *B* Hall plasma thruster. For a prescribed magnetic and electric field distribution in the near-field of a Hall thruster, a staggered leapfrog time-integrating method is utilized to track electrons launched from a simulated cathode. Currently, inter-particle collisions are ignored though collisions with surfaces are treated, and field instabilities are disregarded. Statistics including spatial maps of the relative electron density and mean electron energy as well as electron energy distributions within spatial domains have been obtained.

Nomenclature

$\vec{B}$, $\boldsymbol{B}$	=	magnetic field vector
$\overline{\overline{B}}$	=	magnetic field tensor
β	=	Hall parameter
Δt	=	time step
$\vec{E}$, $\boldsymbol{E}$	=	electric field vector
$\overline{\overline{I}}$	=	unity tensor
m_e	=	electron mass
N_e	=	electron number density
N_{e0}	=	reference electron number density
q	=	fundamental charge
τ_{eff}	=	effective time between collisions
$\vec{V}$	=	electron velocity vector
$V_{\vec{E}x\vec{B}}$,$V_{\boldsymbol{E}x\boldsymbol{B}}$	=	electron velocity component in the $\boldsymbol{E}$ x $\boldsymbol{B}$ direction
$V_{\vec{E}}$,$V_{\boldsymbol{E}}$	=	electron velocity component in the -$\boldsymbol{E}$ direction
ω_{ce}	=	electron-cyclotron frequency
$\vec{x}$	=	electron position vector

[1] PhD Candidate, Mechanical Engineering Department, Stanford University, AIAA Student Member.
[2] Professor, Mechanical Engineering Department, Stanford University, AIAA Member.

I. Introduction

The behavior of the electron current emitted from the cathode of Hall plasma accelerators remains insufficiently described. In a typical co-axial $\boldsymbol{E} \times \boldsymbol{B}$ Hall thruster, such as that illustrated schematically in Fig. 1, approximately 90% of this current serves to neutralize the ion beam, while the remaining 10% migrates into the thruster to service the discharge. However, the details of how electrons migrate across the magnetic field in the near-field (the region between the cathode plane and the discharge channel exit plane) are still poorly understood. Unlike electron transport inside the thruster, which is sometimes attributed to the so-called near-wall conductivity[1,2], there are no plasma-confining walls in the downstream region between the thruster and the external cathode. In simulating the near-field region, a Bohm-model for the electron mobility is often assumed[2] although no direct evidence exists linking transport to plasma fluctuations. A possible alternate explanation for the anomalous electron transport in this region of a Hall discharge that has been surprisingly overlooked is the role played by strong field non-uniformities (in both $\boldsymbol{E}$ and $\boldsymbol{B}$) that can give rise to neoclassical electron transport[3]. An understanding of this phenomenon requires an examination of the electron dynamics in the presence of the non-uniform fields typically found near the exit of Hall thrusters. This paper provides initial insight into this behavior, and shows that these strong nonuniformities can account for the observed electron/ion current and cross-field transport seen in this region of these plasma devices.

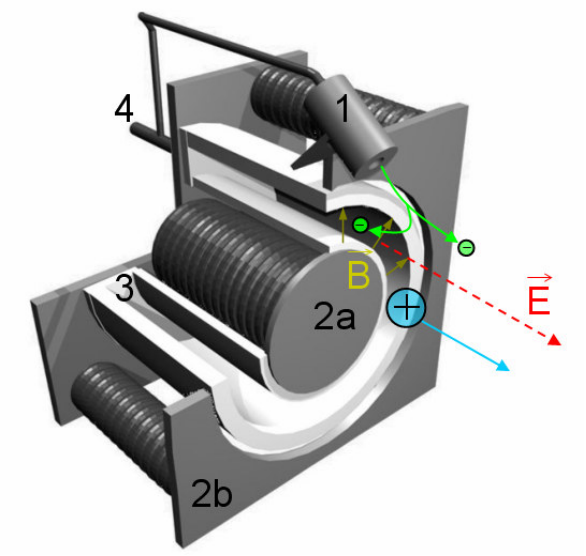

Figure 1. Hall thruster schematic: 1: cathode, 2a/2b: magnetic poles, 3: anode, 4: neutral gas feed line.

II. Simulations

Among the most frequently utilized tools for simulating the discharge and near-field region of Hall thrusters are so-called quasi-neutral hybrid-PIC (Particle-In-Cell) methods in which the electrons are modeled as a fluid continuum and the ions and neutrals are treated kinetically as discrete particles[1,2,4-6]. Such simulations proceed self-consistently with the ion movement influenced by the electric potential, derived from an equation for the average electron velocity, assuming some constitutive relation for the cross-field electron current. It is now widely accepted that the mobility observed inside the discharge channel and near-field is anomalous (i.e., cannot be accounted for by classical electron collisions)[1,7,8], and these simple models often resort to the use of *ad-hoc* transport descriptions such as a mobility that scales as B^{-1}, in accordance with the model of Bohm[9], or equivalently, a constant effective Hall parameter, $\omega_{ce}\tau_{eff}$. While in some cases, one can surmise that secondary electron emission from the dielectric (typically boron nitride – BN) walls of the discharge channels may impact the axial transport of electrons to the anode, in the near-field, as mentioned above, the absence of confining walls suggest the need for an alternative explanation, such as perhaps fluctuation-induced (Bohm-like) transport.

In this study, we show that anomalous transport can be accounted for by the non-local behavior of electron motion due to the strongly non-uniform electric and magnetic fields (neoclassical transport). Such neoclassical charged particle motion is seen in the edge flow of Tokomaks[10,11], where the non-uniform poloidal magnetic field causes so-called ion "banana orbits". The neoclassical motion seen here is attributed to non-uniformities in both $\boldsymbol{E}$ and $\boldsymbol{B}$, and such non-uniformities are common to all modern Hall thruster sources.

Our study focuses primarily on the discrete particle simulations of single electrons in practical Hall thruster configurations. While in principle, full PIC simulations can be carried out with the simultaneous dynamical tracking of a large number of electrons and ions allowing for the electric potential to be solved for self-consistently; such simulations are still intractable for the full geometry of a typical Hall thruster. Instead, we prescribe the electric field, allowing for a relatively smaller number of electrons to be considered. For the results described here, we do not include electron-particle collisions, although in principle, momentum-scattering collisions can be added if the near-field neutral xenon density is known. Electron scattering with external thruster walls are included, although it is found that these scattering events are rare.

The results presented here are dependent on knowledge of the electric field distribution in the near-field of the discharge. Researchers have made measurements of the plasma potential in the near-field and plume of Hall

thrusters[12-14]. While these measurements afford some insight into the structure of the region, most of the measurements are not sufficiently complete to be used in our three-dimensional (3-D) discrete electron transport simulation described below. Instead, our simulations make use of the hybrid-PIC simulations of Tacconga et al for the near-field potential[15,16]. Unlike some hybrid-PIC simulations [e.g., that of Refs. 1, 4] which do not include the region very near the central pole-piece in the computational domain, the results of Refs. 15 and 16 provide a relatively complete plasma potential map for the near-field of an SPT-100 thruster.

For the purpose of our simulations, the calculated exit plane potential is normalized to that measured at the exit of our simulated thruster, which is a 94-mm channel diameter laboratory Hall thruster that has been extensively characterized[17]. The resulting plasma potential distribution for the near-field of this thruster is shown in Fig. 2. At this time, a complete experimental survey of the near-field plasma potential for this thruster has not been made, and it is noted that the data shown in Fig. 2 is unverified experimentally.

The magnetic field structure used in the simulations is assumed to be dominated by the externally applied field of the thruster magnetic circuit. Induced magnetic fields generated by the Hall current are neglected. We make use of FEMM -Finite Element Method Magnetics [18], a finite element magnetic solver in which we have built a model of the Stanford Hall thruster, to obtain this externally applied magnetic field distribution. For the results presented here, the magnetic field is assumed to be axisymmetric, as is the electric field, but this is not a general requirement in the simulation, and can be lifted in future studies.

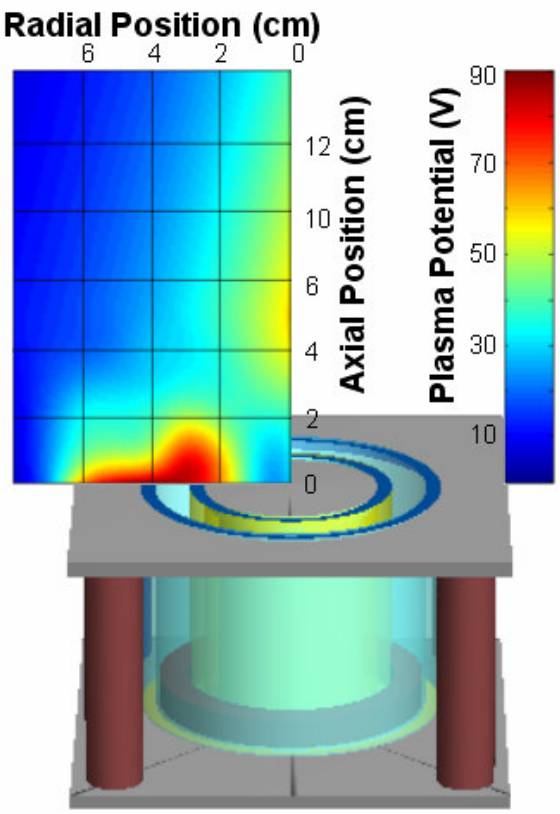

Figure 2 Plasma potential map superimposed above a model of the Stanford Hall thruster.

In the simulation, electrons released from a point representing a virtual cathode are tracked until they exit the simulation domain which extends parallel to the exit plane 30 cm outward from the central axis and 30 cm outward from the exit plane along the central axis. The particles are tracked using a staggered leapfrog integrator following Birdsall and Langdon[19] for the equations of motion, but various methods have been tested for comparison[20,21].

In this paper, the usefulness of such a simulation is evaluated in terms of its ability to yield information concerning the electron transport in the near-field while matching typical values for the ratio of channel to beam current found experimentally. Results of the position-distribution, energy-distribution, and local Hall parameter are also presented.

Applying a staggered leapfrog method to the equations of motion gives us the time advancement in the electron velocity and position:

$$\vec{V}_{t+\Delta t/2} = -\frac{q\Delta t}{m_e}\left(\vec{E} + \vec{V} \times \vec{B}\right)_t + \vec{V}_{t-\Delta t/2} \tag{1}$$

$$\vec{x}_{t+\Delta t} = \Delta t \vec{V}_{t+\Delta t/2} + \vec{x}_t \tag{2}$$

Here, $\vec{V}$, $\vec{x}$, $\vec{E}$, and $\vec{B}$ are the velocity, position, electric field, and magnetic field vectors respectively, q is the fundamental charge, m_e is the electron mass, and the subscripts denote the time step at which each variable is evaluated with Δt as the time step. With this formulation, one problem which arises concerns the treatment of the velocity-dependent Lorentz force on the electrons. Determining this force requires knowledge of the electron

velocity at a time, *t*, for which it is not explicitly calculated. Here, we apply the linear approximation proposed by Buneman[22]:

$$\vec{V}_t \approx \frac{\vec{V}_{t+\Delta t/2} + \vec{V}_{t-\Delta t/2}}{2} \tag{3}$$

Substitution into Eq. 1 yields:

$$\vec{V}_{t+\Delta t/2} = -\left(\bar{\bar{I}} + \frac{q\Delta t}{2m_e}\bar{\bar{B}}_t\right)^{-1} \frac{q\Delta t}{m_e}\vec{E}_t + \left(\bar{\bar{I}} + \frac{q\Delta t}{2m_e}\bar{\bar{B}}_t\right)^{-1}\left(-\bar{\bar{I}} - \frac{q\Delta t}{2m_e}\bar{\bar{B}}_t\right)\vec{V}_{t-\Delta t/2} \tag{4}$$

where

$$\bar{\bar{I}} = \begin{bmatrix} 1 & 0 & 0 \\ 0 & 1 & 0 \\ 0 & 0 & 1 \end{bmatrix} \quad and \quad \bar{\bar{B}}_t = \begin{bmatrix} B_x & 0 & 0 \\ 0 & B_y & 0 \\ 0 & 0 & B_z \end{bmatrix}_t \tag{5}$$

Implementation of Eq. 4 will be referred to from here on as the Buneman-Leapfrog Method (BLM). For the results presented here, an adaptive time-step is utilized, with the time-step selected to be 0.1% of the local cyclotron orbital period. We have found that this adaptive time step affords a high degree of accuracy in regions of strong magnetic field, while greatly enhancing the speed of calculations when the electrons travel away from the exit plane where the magnetic field strength drops rapidly.

III. Simulation Results

The simulation results fall into four categories: global current transport statistics, spatial maps of relative electron density and energy, spatial maps of the computed Hall parameter, and local energy distributions. In all cases the simulated cathode was positioned at a point 7.07 cm radially outward from the central axis and 2 cm axially outward from the exit plane because this represented the location of the cathode position on the real thruster. The electrons were emitted in all directions from the virtual cathode with a distribution of energies about a mean of 0.2 eV. The cathode was located at a position where the plasma potential was 19.2 V, and no sheath model was implemented to this point so the electron are not treated as accelerating through any potential drop before exiting the cathode.

A. Global current-transport statistics

The global current-transport statistics refer to the overall distribution of electron current from the cathode. There are only two classes of electrons at this level. As each electron leaves the simulation domain, its terminal position is stored. Those electrons which exit the simulation at the location of the thruster channel are stored as "channel" electrons, and all others are stored as "plume" electrons. Table 1 below shows the resulting overall statistics. The results are shown for two different time-steps to illustrate that the simulation is insensitive to time-step within this range.

	Electron Current		Plume/Channel
$\Delta t^*\omega_{ce}$	Plume (%)	Channel (%)	Current Ratio
0.01	88.36	10.21	8.65:1
0.05	89.36	10.63	8.41:1

Table 1. Global electron current statistics for calculations made with the BLM.

On average, slightly less than 90% of the electrons emitted at the cathode leave the simulation domain in the plume, and the remaining 10% or so are seen to leave the simulation domain at the thruster channel in agreement with experimental observations.

B. Spatial maps of relative electron density and energy

By discretizing the simulation domain into smaller volumes and tracking the transient position and velocity of the electrons as they migrate, spatial maps of the relative electron density and mean energy can be created. Every virtual nanosecond the positions, velocity components, and energies of the electrons were cataloged in each cell.

Statistics were established in cells located within 3 spatial planes as illustrated in Fig. 3. The first two planes are parallel to the exit plane of the thruster and extend 10 cm from the central axis in both the x- and y-directions. The third plane is oriented parallel to the central axis and set at x = 0. This orientation was chosen to investigate the symmetry on either side of the cathode. Planes 1 and 2 are discretized into cells 2.5 mm on a side in the x- and y-direction and 5 mm in the z-direction with a resulting volume of 31.25 mm^3 each. Planes 1 and 2 span a thickness from z = 0 mm to 5 mm and z = 7.5 mm to 12.5 mm respectively. Plane 3 extends radially outward 15 cm in the positive and negative y-directions and 30 cm in the z-direction. It is discretized into cells 2.5 mm on a side in the y- and z-direction and 5 mm on a side in the x-direction (2.5 mm in the positive and negative x-direction) with a resulting volume of 31.25 mm^3.

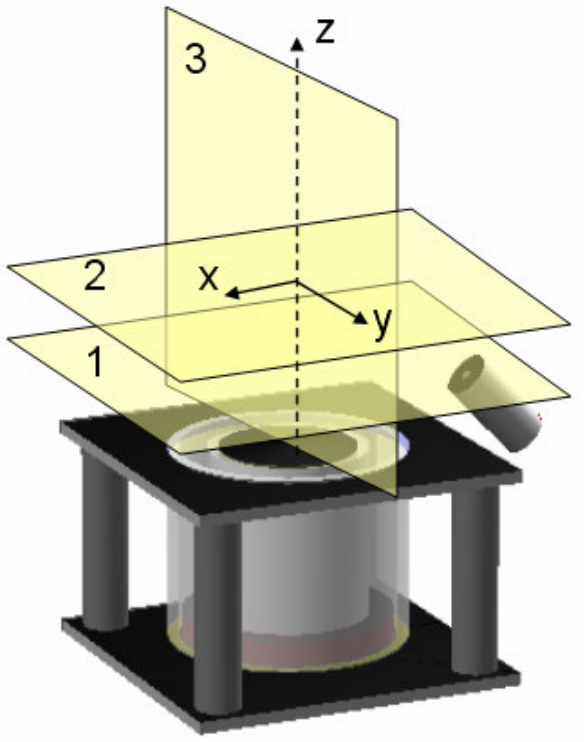

Figure 3. Schematic of spatial planes for which electron density and energy statistics have been computed.

Reference cells were chosen at x = 4 cm, y = 0 cm, and z = 0 cm for planes 1 and 3 and at x = 4 cm, y = 0 cm, and z = 1 cm for plane 2. The numbers of electrons in the cells were normalized by the number of electrons cataloged in these reference cells to produce maps of the relative electron number density N_e/N_{eo}. The total relative electron number density in planes 1, 2, and 3 are shown in Figs. 4, 5, and 10, respectively.

Since the electrons were tracked for the full extent of their lifetime in the domain, it was possible to separate out the histories of those electrons which eventually ended up exiting the domain in the channel of the thruster. Figure 6 illustrates the relative number density of electrons in plane 1 which eventually end up reaching the channel of the thruster. The relative number density of electrons in plane 2 which eventually end up reaching the channel is shown in Fig. 7. Plane 3 is not shown because too few electrons which eventually reached the channel occupied most of these cells to have significant statistics computed to this point.

Along with the total number of electrons, the energy of each electron in each cell was cataloged every virtual nanosecond. At the end of the simulation, the electron energies in each cell were averaged to produce spatial maps of the mean electron energy in addition to the relative number density. Figures 8, 9, and 11 show color maps of the computed mean electron energy in planes 1, 2, and 3, respectively. It is evident in these figures that the electron energy is particularly high along the central axis of the thruster. An examination of Figs. 4, 5, and 10 indicate that there is generally a lower density of electrons along the central axis in the near field. However, these electrons are seen to possess a considerably larger mean energy. As discussed below, some of these electrons have anomalously high energy. We refer to these electrons as anomalous if they possess energies outside the range predicted by energy conservation. While some (few) of these electrons can be created as a result of collisions with surfaces (where energy is not conserved, rather, the electrons are reemitted with an energy set by the temperature of the surface they collide with). We believe that the majority of these electrons must arise due to errors in the simulation itself, possibly due to the discretized nature of the electric field used.

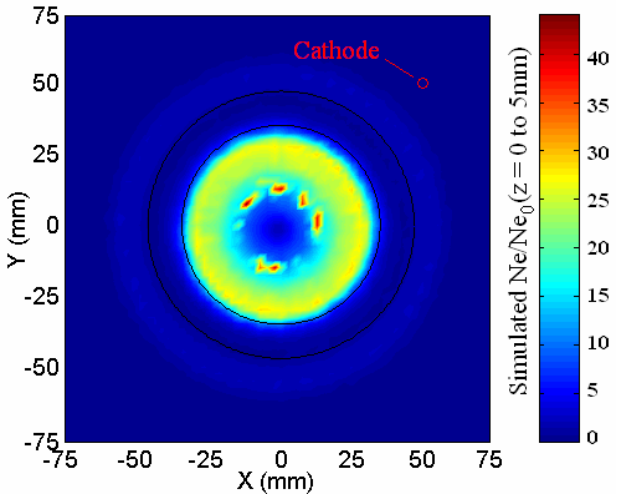

Figure 4. Simulated total relative electron number density in plane 1 (z = 0 mm to 5 mm).

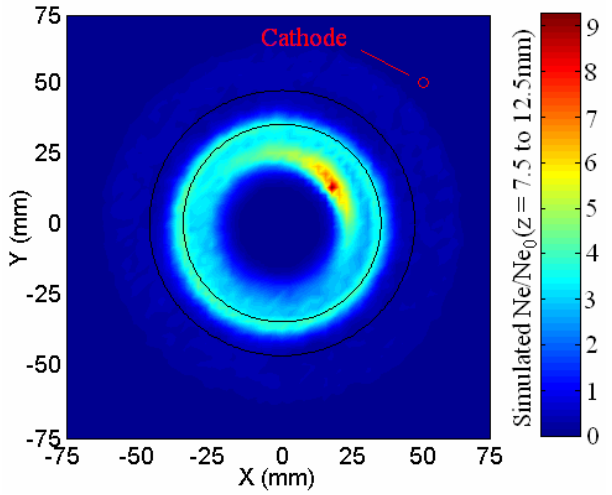

Figure 5. Simulated total relative electron number density in plane 2 (z = 7.5 mm to 12.5 mm).

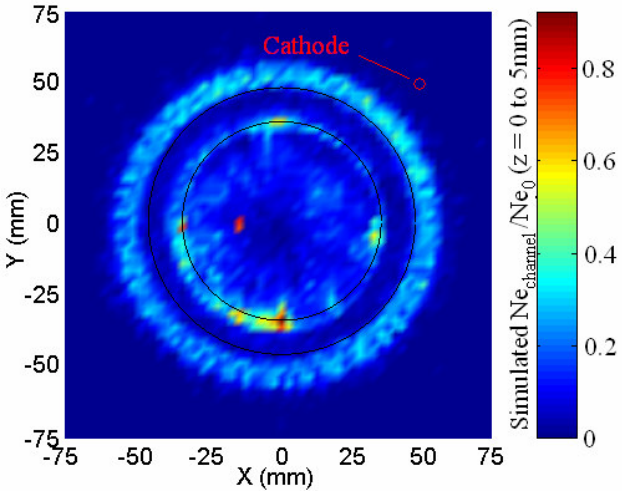

Figure 6. Simulated relative number density of electrons in plane 1 (z = 0 mm to 5 mm) exiting the domain into the thruster channel.

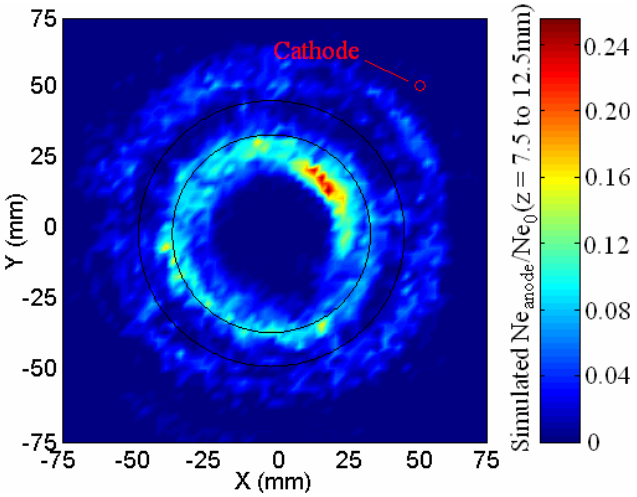

Figure 7. Simulated relative number density of electrons in plane 2 (z = 7.5 mm to 12.5 mm) exiting the domain into the thruster channel.

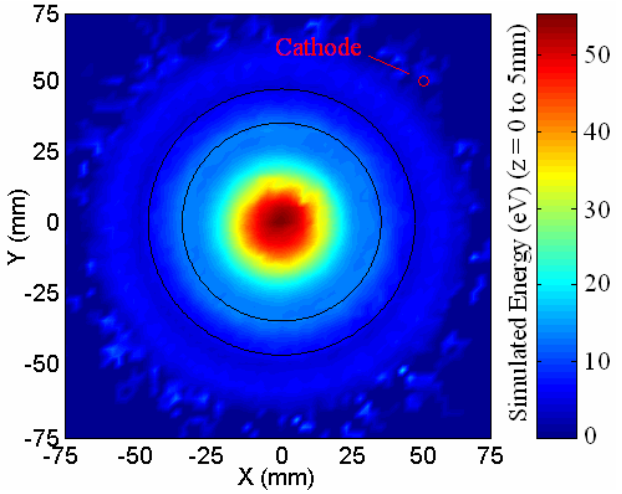

Figure 8. Simulated mean electron energy in plane 1 (z = 0 mm to 5mm)

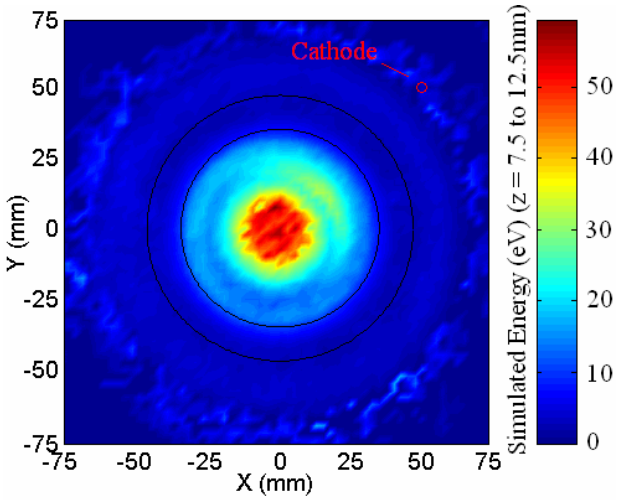

Figure 9. Simulated mean electron energy in plane 2 (z = 7.5 mm to 12.5 mm)

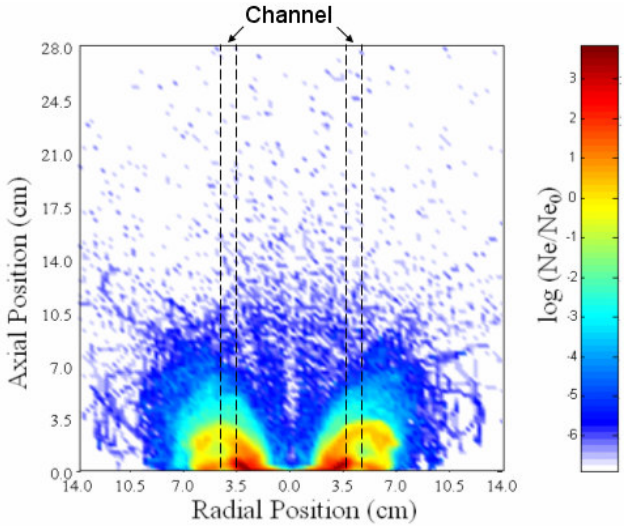

Figure 10. Simulated total relative electron number density in plane 3

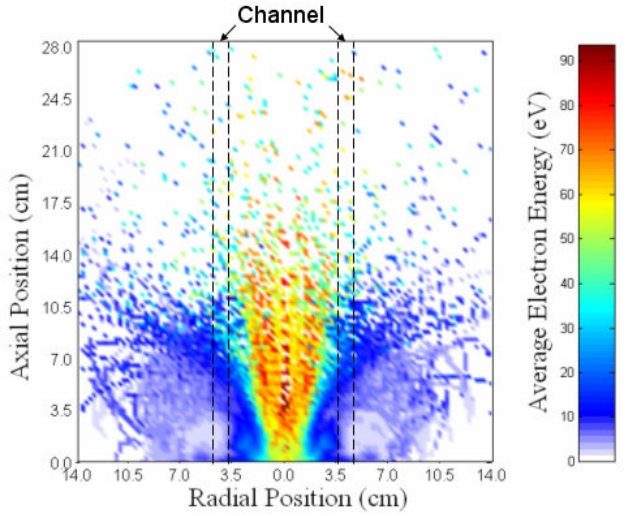

Figure 11. Simulated mean electron energy in plane 3

C. Spatial map of Hall parameter

In addition to the energy and relative number density statistics, an estimation of the local Hall parameter can be obtained from the simulation. When the electron energies and positions are cataloged, the components of their velocity in the local ***E***- and ***E*** x ***B***-directions are stored. The estimated Hall parameter, β, is then defined as the ratio of the components of velocity as:

$$\beta = \frac{V_{\vec{E}x\vec{B}}}{V_{\vec{E}}} \tag{6}$$

where V_{ExB} is the electron velocity component in the ***E*** x ***B*** direction, and V_E is the velocity component in the ***E*** direction. After the simulation is complete, the set of Hall parameter values within each cell is averaged. A spatial map of the computed local Hall parameter (on a logarithmic scale) is shown in Fig. 12 at right. The radial boundaries of the channel are shown with red dashed lines. The global average Hall parameter value was found to be 1.08. Fewer tests were completed for computing the local Hall parameter, so only part of the results from plane 3 are shown.

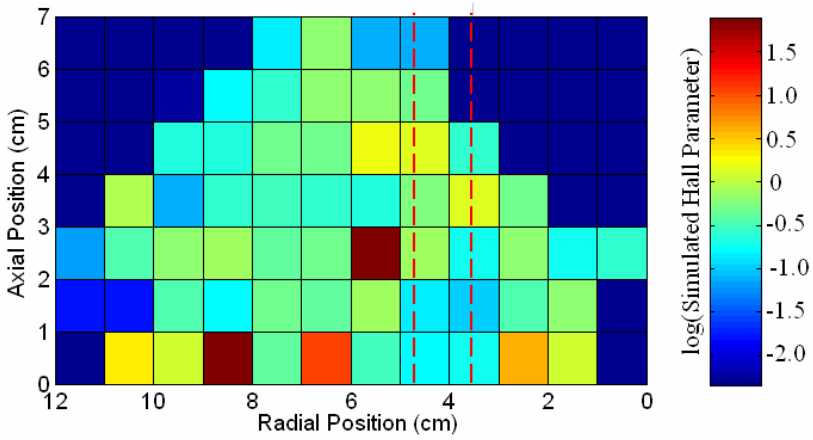

Figure 12. Simulated local Hall parameter in a portion of plane 3

D. Local energy distributions

Each of the electrons in a given cell possesses a unique energy. By cataloging the individual electron energies in a given spatial cell, a local energy distribution is computed as statistics are accumulated. Figure 13 shows the total electron energy distribution; that is, the sum of all the individual cells' energy distributions. Given that the electrons are released with a small energy (0.2 eV) at the cathode, which is situated at a 19.2 V potential, and the maximum potential in the domain is 90 V, the maximum possible energy accessible to the electrons is approximately 70 eV. It is clear from the overall distribution in Fig. 13 that some electrons possess energies in excess of this theoretical limit. While only 1.49% of the electrons possess anomalously high energy when the overall global distribution is considered, the distributions within individual cells sometimes have a larger fraction of anomalous electrons. For

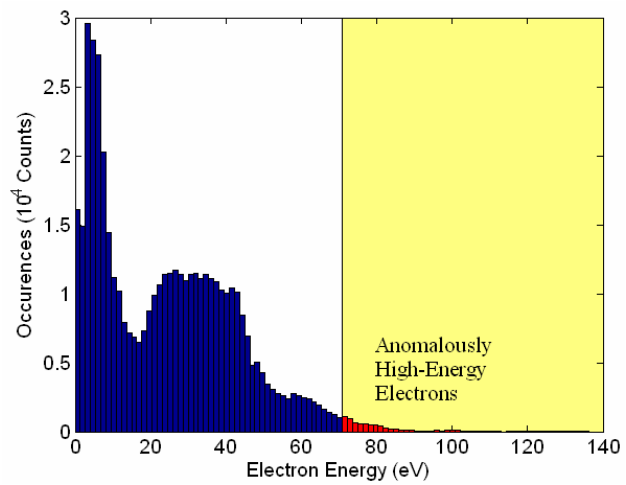

Figure 13. Overall energy distribution of electrons in the simulation.

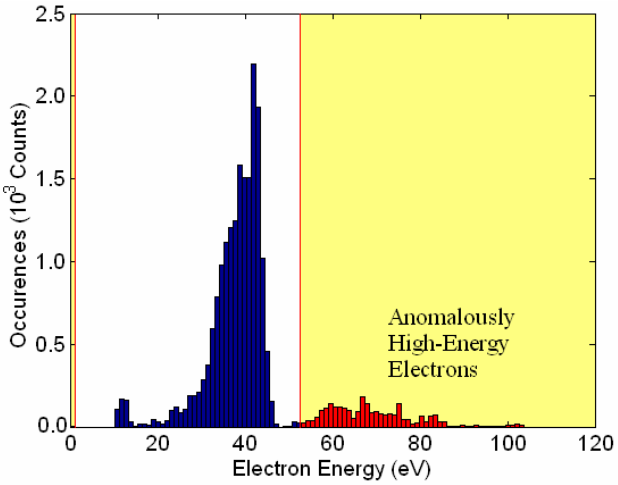

Figure 14. Electron energy distribution within the spatial cell bounded by x,y = -4 cm to -5 cm, z = 0 cm to 1 cm.

establishing these individual energy distributions, spatial cells 1 cm on a side (with a resulting volume of 1 cm^3) were established. The allowable range of energies is based on the variation of the plasma potential within the spatial cell. The electrons may not possess energies greater than the difference between the maximum plasma potential in the cell and the potential from which they were release at the cathode (plus a small initial energy). Furthermore, they may not possess energies less than the minimum difference between the plasma potential and the cathode potential (neglecting those electrons that have been reemitted after a collision with a surface). Electrons with energies outside the range allowed by energy conservation are considered anomalous. The energy distributions within two spatial cells are shown: Fig. 14 shows the electron energy distribution in the cell which extends from x = -4 cm to -5 cm, y = -4 cm to -5 cm, and z = 0 cm to 1 cm, and Fig. 15 shows the electron energy distribution x = -4 cm to -5 cm, y = -3 cm to -4 cm, and z = 0 cm to 1 cm. The fraction of anomalous electrons is 0.102 (10%) in Fig. 14 which is greater than the global average, and the fraction of anomalous electrons in Fig. 15 is 0.0138 (1.38%).

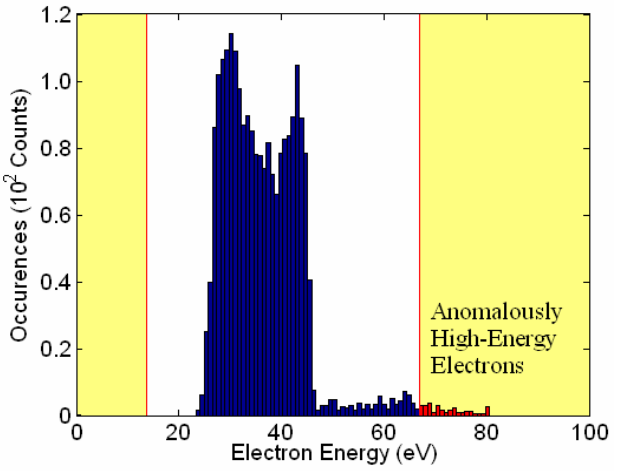

Figure 15. Electron energy distribution within the spatial cell bounded by x = -4 cm to -5 cm, y = -4 cm to -3 cm, z = 0 cm to 1 cm.

IV. Conclusion

Considering the initial approximations in this approach, the quantitative results should be accepted with caution; however, if the measured electric potential for the studied thruster turns out to nearly match the current estimate, then some qualitative conclusions can be inferred from the results. The effect of a discrete electric field mesh is problematic in that it introduces the possibility for anomalous energies to be obtained by the electrons in the simulation. However, these anomalous electrons constitute a relatively small fraction of the whole. The first conclusion that may be drawn from the results in this paper is that the necessity for fluctuation-induced (Bohm) diffusion of electrons across the magnetic field lines in the near field may be overstated. Global current statistics computed by only treating neoclassical electron transport indicate that the strong field nonuniformities in the near field may be sufficient to drive the observed current. Second, the preliminary data suggest an estimate for the near-field Hall parameter of ~1 which is considerably lower than the Bohm value. This Hall parameter appears anisotropic, however, and certain regions in the near-field do possess large Hall parameter values. Finally, the spatial maps of relative electron density and mean energy indicate that the region of the near field along the central

axis, while deficient in electrons, possesses high energy electrons that may be responsible for the excitation and light emission that is frequently present in this region.

Acknowledgments

The authors thank the Air Force Office of Scientific Research for financial support, and A. W. Smith thanks the National Defense Science and Engineering Graduate Fellowship program for its financial support as well.

References

[1]Fife, J.M.,"Hybrid-PIC Modeling and Electrostatic Probe Survey of Hall Thrusters," Ph.D. Dissertation, Aeronautics and Astronautics Dept., Massachusetts Institute of Technology, Cambridge, MA, 1998.

[2]Hagelaar, G. J. M., Bareilles, J., Garrigues, L., and Boeuf, J. -P., "Two-dimensional model of a stationary plasma thruster", J. of Appl. Phys. 91, pp. 5592-5598, 2002.

[3]Thomas, C., "Anomalous electron transport in the Hall effect thruster," Ph.D. Thesis, Stanford University, 2007.

[4]Scharfe, M. K. Gascon, N. and Cappelli, M. A., "Comparison of hybrid Hall thruster model to experimental measurements", Phys. Plasmas 13, 083505, 2006.

[5]Fife, J. M., Martinez-Sanchez, M., and Szabo, J., "A numerical study of low-frequency discharge oscillations in Hall thrusters", AIAA-1997-3052 , 33rd AIAA Joint Propulsion Conference, Seattle, WA, July 6-9, 1997.

[6]Hagelaar, G. J. M., Bareilles, J., Garrigues, L., Boniface, C., Boeuf, J. P., and Gascon, N., "Critical assessment of a two-dimensional hybrid Hall thruster model: Comparisons with experiments" Phys. Plasmas 11, pp. 3035-3046, 2004.

[7]Meezan, N.B., Hargus, W.A. Jr., and Cappelli, M.A. "Anomalous electron mobility in a coaxial Hall discharge plasma, Phys. Rev. E 63, 026410, 2001.

[8]Choueiri, E., "Plasma oscillations in Hall thrusters, Phys. Plasmas 8, pp. 1411-1426, 2001

[9]Bohm, D., in *The Characteristics of Electrical Discharges in Magnetic Fields*, edited by A. Guthrie and R. K. Wakerling McGraw-Hill, New York, 1949, Chap. 2, p. 65.

[10]Chen.F, in *Introduction to Plasma Physics*, Plenum Press, 1974.

[11]Lotz, W., and Nührenberg, J., "Monte Carlo computations of neoclassical transport," Physics of Fluids 31, pp. 2984-2991, 1998.

[12]Smirnov, A., Raitses, Y., and Fisch, N. J., "Plasma Measurements in a 100W Cylindrical Hall Thruster," *Journal of Applied Physics*, Vol. 95, Num. 5, 2004, pp. 2283-2292.

[13]King, L.B., "Transport Property and Mass Spectral Measurements in the Plasma Exhaust Plume of a Hall-effect Space Propulsion System," Ph.D. Dissertation, Department of Aerospace Engineering, University of Michigan, Ann Arbor, MI, 1998.

[14]Hofer, R. H., and Gallimore, A. D., "Recent Results From Internal and Very-Near-Field Plasmas Diagnostics of a High Specific Impulse Hall Thruster", NASA/CR – 2003-212604, IEPC-2003-037, 2003.

[15]Tacconga, F., Longo, S., Capitelli, M., "Very-Near-Field Plume Simulation of a Stationary Plasma Thruster," *Applied Physics proofs*, 2004.

[16]Tacconga, F., Longo, S., Capitelli, M., "Very-Near-Field Plume Simulation of a Hall Thruster".

[17]Hargus, W. A., Jr., "Investigation of the Plasma Acceleration Mechanism within a Coaxial Hall Thruster," Ph.D. Dissertation, Department of Mechanical Engineering, Stanford University, Stanford, CA, 2001.

[18]FEMM, Finite Element Method Magnetics, Software Package, Version 4.0, David Meeker, 2004.

[19]Birdsall, C.K., and Langdon, A.B. "Plasma Physics Via Computer Simulation," Institute of Physics Publishing, Bristol and Philadelphia, 1991.

[20]Smith, A. W., and Cappelli, M. A., "Investigation of Field Structure and Electron Behavior in the Near-Field of Hall Thruster",AIAA-2006-4835, 42nd AIAA/ASME/SAE/ASEE Joint Propulsion Conference and Exhibit, Sacramento, California, July 9-12, 2006

[21]Moin, P., "Fundamentals of Engineering Numerical Analysis," Cambridge University Press, 2001.

[22]Buneman, O., "Time Reversible Difference Procedures," *Journal of Computational Physics*, Vol. 1, 1967, pp. 517-535.